6276 *Biochemistry* **2010,** *49,* 6276–6281
DOI: 10.1021/bi1006699

BIOCHEMISTRY
including biophysical chemistry & molecular biology
Article

Functional and Structural Impact of Target Uridine Substitutions on the H/ACA Ribonucleoprotein Particle Pseudouridine Synthase[†,‡]

Jing Zhou,[§] Bo Liang,[∥] and Hong Li*[,§,∥]

[§]*Department of Chemistry and Biochemistry and* [∥]*Institute of Molecular Biophysics, Florida State University, Tallahassee, Florida 32306*

Received April 30, 2010; Revised Manuscript Received June 23, 2010

ABSTRACT: Box H/ACA ribonucleoprotein protein particles catalyze the majority of pseudouridylation in functional RNA. Different from stand alone pseudouridine synthases, the RNP pseudouridine synthase comprises multiple protein subunits and an RNA subunit. Previous studies showed that each subunit, regardless its location, is sensitive to the step of subunit placement at the catalytic center and potentially to the reaction status of the substrate. Here we describe the impact of chemical substitutions of target uridine on enzyme activity and structure. We found that 3-methyluridine in place of uridine inhibited its isomerization while 2′-deoxyuridine or 4-thiouridine did not. Significantly, crystal structures of an archaeal box H/ACA RNP bound with the nonreactive and the two postreactive substrate analogues showed only subtle structural changes throughout the assembly except for a conserved tyrosine and a substrate anchoring loop of Cbf5. Our results suggest a potential role of these elements and the subunit that contacts them in substrate binding and product release.

The box H/ACA ribonucleoprotein particles (RNPs) comprise the most complex pseudouridine synthases that are required for modification of ribosomal and spliceosomal RNAs (*1*−*5*). Elucidating the function of box H/ACA RNPs has important implications in studies of ribosome and spliceosome biogenesis and diseases associated with their dysfunction. In humans, a box H/ACA RNP has a minimum of four proteins (DKC1 or dyskerin, NOP1, NHP2, and GAR1) and a small RNA. The RNA subunit specifies the substrate RNA via base complementarity while the proteins catalyze the actual pseudouridylation reaction. The rare genetic disorder, dyskeratosis congenita (DC), is correlated with single site mutations primarily on the catalytic subunit of human RNA-dependent pseudouridine synthase, dyskerin, and some also on NOP1 and NHP2 (*6*−*9*). Furthermore, pseudouridine synthases are strongly inhibited by 5-fluorouracil-substituted RNA substrates (*10*). 5-fluorouracil is a common chemotherapeutic drug that is effective on colorectal and breast cancers (*11*). Although a direct correlation between the antiproliferation effect of 5-fluorouracil and pseudouridine synthase function has not been established, 5-fluorouridine is known to be incorporated into cellular RNA molecules (*12*−*14*). Precisely how the uracil nucleobase influences pseudouridine synthase structure and function, and consequently disease development or therapy, remains unclear.

Previous structural studies of archaeal homologues of box H/ACA RNPs (proteins are correspondingly Cbf5, Nop10, L7Ae, and Gar1) revealed the overall organization of the enzyme (Figure 1A) (*15*−*18*). The box H/ACA RNPs comprise the most complicated pseudouridine synthase owing to the large assemblage of five enzymatic subunits. Cbf5 is the key subunit that both organizes the assembly of the RNP and catalyzes the isomerization process. The H/ACA RNA, also termed guide RNA, binds the substrate RNA targeted for modification via base pairing. Both Nop10 and L7Ae participate in binding the guide RNA, which, in turn, places the substrate RNA into the active site (Figure 1A). The Gar1 protein does not interact with either RNA but is known to enhance catalytic activity (*19*). However, these conclusions are derived only from structural studies with a substrate containing 5-fluorouridine that is known to be converted by the enzyme to 5-fluoro-6-hydroxypseudouridine (5FhΨ). In the case of other bacterial pseudouridine synthases, 5FhΨ is believed to be covalently linked to the enzyme and is therefore a strong inhibitor of these enzymes. Thus, possible structural transitions throughout the entire reaction pathway remain elusive. In the present work, we constructed three substrate analogues that contain 3-methyluridine (3MU), or 2′-deoxyuridine (2dU), or 4-thiouridine (4SU) in place of the target uridine (Figure 1B). We studied their reactivity to the hyperthermophile archaeon *Pyrococcus furiosus* (Pf) H/ACA RNP and obtained their crystal structures in complex with the H/ACA RNP enzyme. The structures containing nonreactive analogues provide views of the enzyme before reaction while those containing reactive analogues provide views after reaction. Together with previously known structures, our results reveal specific structural transitions of the enzyme along the reaction pathway and suggest important roles of a substrate anchoring loop, and potentially Gar1, in the release of reaction product.

[†]This work was supported in part by National Institutes of Health Grant R01 GM66958-01 (H.L.). J.Z. is a predoctoral fellow of the American Heart Association, Florida/Puerto Rico Affiliate (0815267E). B.L. is a predoctoral fellow of the American Heart Association, Florida/Puerto Rico Affiliate (0415179B). X-ray diffraction data were collected from the Southeast Regional Collaborative Access Team (SER-CAT) 22-ID beamline at the Advanced Photon Source, Argonne National Laboratory. Use of the Advanced Photon Source was supported by the U.S. Department of Energy, Office of Science, Office of Basic Energy Sciences, under Contract W-31-109-Eng-38.

[‡]Coordinates and structure factors have been deposited in the Protein Data Bank with accession numbers 3LWQ (3MU), 3LWR (4SU), and 3LWV (2dU).

*To whom correspondence should be addressed. E-mail: hong.li@fsu.edu. Phone: (850) 644-6785. Fax: (850) 644-7244.

 Published on Web 06/24/2010

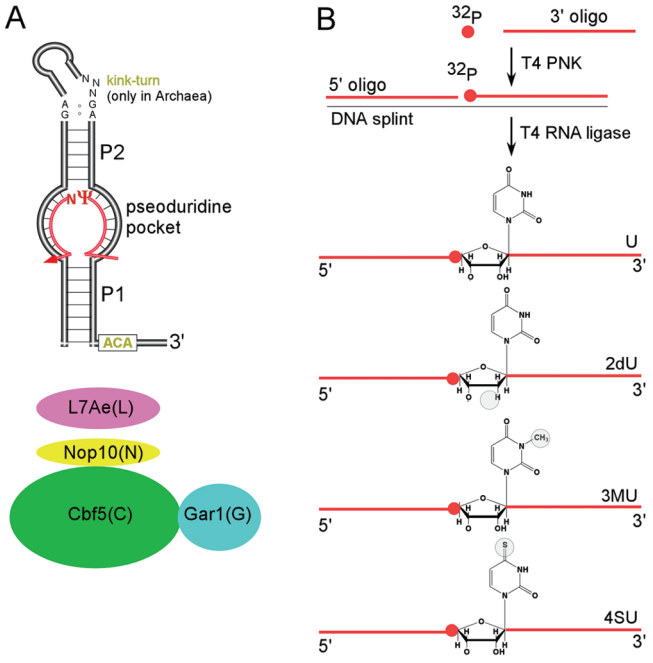

FIGURE 1: (A) Cartoon representation of the archaeal box H/ACA ribonucleoprotein particle pseudouridine synthase. Each subunit is also abbreviated by a single letter code. Key secondary elements of the guide RNA (upper) are labeled. The red strand represents a bound substrate RNA. (B) Schematics of the DNA splint method for generating substrates containing isotope-labeled and modified uridine. "T4 PNK" stands for T4 polynucleotide kinase.

MATERIALS AND METHODS

Protein Expression, Purification, and Crystallization. *P. furiosus* H/ACA RNP components were prepared as previously described (*15*, *17*, *20*). Substrate 22mer RNA 5′-rGrArUrGrGrArGrCrGXrGrCrGrGrUrUrUrArArUrG-3′, where X is 2dU, 4SU, or 3MU, were ordered from Dharmacon (Chicago, IL) or IDT (Coralville, IA) and purified according to the manufacturers' protocols. For crystallization, guide RNA and substrate RNA were first combined at a molar ratio of 1:1 and then combined with Cbf5, Nop10, and L7Ae at 1:1:1 molar ratio to a final protein total concentration of 20 mg/mL. The complex was then incubated at 70 °C for 30 min and allowed to cool to 25 °C. Crystals were obtained after 3 days in 0.2 M KCl, 0.15 M magnesium acetate, 8% PEG 6000, and 50 mM sodium cacodylate, pH 6.5 at 30 °C, by hanging-drop vapor diffusion. The crystals were soaked in a cryosolution (1.2 M KCl, 0.3 M NaCl, 0.15 M magnesium acetate, 8% PEG 6000, and 50 mM sodium cacodylate, pH 6.5) for 10 min before being flash-cooled under a liquid nitrogen stream. Diffraction data were collected at Southeast Regional Collaborative Access Team (SER-CAT) 22ID and 22BM beamlines at Argonne National Laboratory and were processed by HKL2000 (*21*).

Structure Determination. The structures were solved by molecular replacement using Molrep (*22*). The published coordinates for the 5FhΨ complex structure (*15*) were used as the search model. The substrate RNA was omitted in the initial model in order to avoid model bias. At later stages of refinement, computed $3F_o - 2F_c$ density maps phased with proteins and the guide RNA allowed 3MU-containing substrates to be built by COOT (*23*) and O (*24*). Electron density maps at the active sites of 2dU and 4SU complexes showed the modified bases are disordered. All structures were refined by PHENIX (*25*). The figures were prepared using PYMOL (*26*). Data collection and refinement statistics are included in Table 1.

Pseudouridylation Activity Assay. In order to achieve site-specific labeling of the target nucleotide, we employed the DNA splint method in which the 22mer substrates were generated by ligation of two half-oligos (*27*), 5′-rGrGrArUrGrGrArGrCrG-3′ and 5′-XrGrCrGrGrUrUrUrArArUrG-3′, where X is 2dU, 4SU, or 3MU, that were purchased from Dharmacon (Chicago, IL) and IDT (Coralville, IA). Ligation was performed using the T4 DNA ligase (Invitrogen, Carlsbad, CA) and a DNA template, 5′-CATTAAACCGCACGCTCCATCTATAGTGAGTCGTATTAAATTC-3′ (IDT, Coralville, IA). The 30mer DNA substrate (DNA2dU) was generated by ligation of 5′-GCTATAGATGGAGCG-3′ and 5′-XGCGGTTTAATGTTG-3′, where X is 2dU. The modified nucleotides X were labeled at the 5′ end with [γ-^{32}P]ATP (PerkinElmer, Waltham, MA) by a T4 polynucleotide kinase reaction (NEB, Ipswich, MA) according to the manufacurer's protocol. The H/ACA RNP components (total protein at 3 μM and H/ACA RNA at 2.5 μM) were first incubated at 70 °C for 5 min in a reaction buffer containing 100 mM Tris-HCl, pH 8.0, 100 mM ammonium acetate, 5 mM $MgCl_2$, 2 mM DTT, and 0.1 mM EDTA before adding the labeled substrates. The reaction mix continued to be incubated for an additional 2 h. The labeled substrates were then purified by phenol extraction and ethanol precipitation and digested by nuclease P1 into nucleotides. The digested nucleotides were analyzed by thin-layer chromatography as previously described (*4*).

RESULTS

Effects of Uridine Modification on Its Isomerization. The previously known structure of H/ACA RNP pseudouridine synthase bound with 5FhΨ-containing RNA substrate revealed the mode of 5FhΨ binding to the active site (*15*, *16*) and suggested possibilities for the active site to accommodate other modified uridine. In order to study how uridine modifications impact the chemical steps of isomerization reaction and the enzyme structure, we incorporated 3-methyl (3MU), 2′-deoxy (2dU), and 4-thio (4SU) modified uridine into a 22mer substrate for the Pf H/ACA RNP pseudouridine synthase (Figure 1B). We also incorporated 2′-deoxyuridine into the 30mer substrate comprised of all deoxynucleotides (DNA2dU). To carry out pseudouridylation assay on the substrates containing modified uridines, we used the DNA splint technique for constructing substrate RNA from two synthetic oligos (*27*) with a ^{32}P label on the 5′ position of the target uridine or modified uridines (Figure 1B). The integrity of the ligated substrate RNA was checked on a denaturing polyacrylamide gel (Supporting Information Figure S1). After pseudouridylation assays with saturating amount of H/ACA RNP synthase and nuclease P1 digestion of RNA substrates, formation of uridine (or modified uridine) isomers was detected by thin-layer chromatography.

The substrate containing 2dU or 4SU was isomerized while that containing 3MU or DNA2dU was not (Figure 2). Compared to WT substrate, an obvious reduction in the amount of isomerized product from the 2dU and 4SU substrates was observed, suggesting an important, although nonessential, role played by the 2′-hydroxyl and 4-oxy groups in catalysis (Figure 2). Similarly to previous enzyme activity assay and structural results, the H/ACA RNP without Gar1 was also functional on WT, 2dU, or 4SU substrate (Figure 2). The result that DNA2dU did not support isomerization is expected because it would form an RNA−DNA hybrid duplex with the guide RNA that may significantly disrupt the orientation of the bound substrate. The result that 3MU

Table 1: Data Collection and Refinement Statistics

	2dU	4SU	3MU
data collection			
space group	$P2_12_12$	$P2_12_12$	$P2_12_12$
cell dimensions			
a (Å)	186.8	187.3	187.1
b (Å)	64.3	64.4	63.7
c (Å)	83.4	83.4	81.9
α, *β*, *γ* (deg)	90, 90, 90	90, 90, 90	90, 90, 90
resolution range (Å)	50.0−2.60 (2.69−2.60)	100.0−2.30 (2.34−2.30)	50.0−2.70 (2.80−2.70)
R_{sym}	0.155 (0.54)	0.101 (0.566)	0.11 (0.592)
$I/\sigma(I)$	47.8 (3.6)	37.5 (5.7)	34.8 (3.7)
redundancy	12.9 (7.7)	10.3 (10.1)	6.6 (5.9)
completeness (%)	98.7 (91.3)	99.7 (99.3)	86.1 (99.9)
refinement			
resolution range (Å)	34.64−2.60	41.70−2.30	32.32−2.70
no. of unique reflections	31310	45289	23711
R_{work}/R_{free}	20.58/24.39	20.65/24.45	21.70/28.81
no. of amino acid/nucleotide	500/71	500/71	496/71
no. of protein/RNA atoms	3882/1512	3882/1513	3844/1514
no. of waters/ions	2/1	57/1	14/1
B-factors			
Cbf5/Nop10/L7ae	73.1/76.4/94.5	31.8/35.1/54.5	67.2/69.2/103.6
guide RNA/substrate RNA	98.1/162.6	57.6/118.1	101.4/160.1
ion/water	325.3/64.1	120.7/25.4	317.6/55.8
rms deviation of the model			
bond length (Å)	0.006	0.006	0.011
bond angle (deg)	1.074	1.027	1.521
Ramachandran plot (%)			
in most favored region	91.3	93.5	89.1
in additionally allowed region	8.2	6.2	10.4
in generously allowed region	0.5	0.2	0.5
in disallowed region	0.0	0.0	0.0

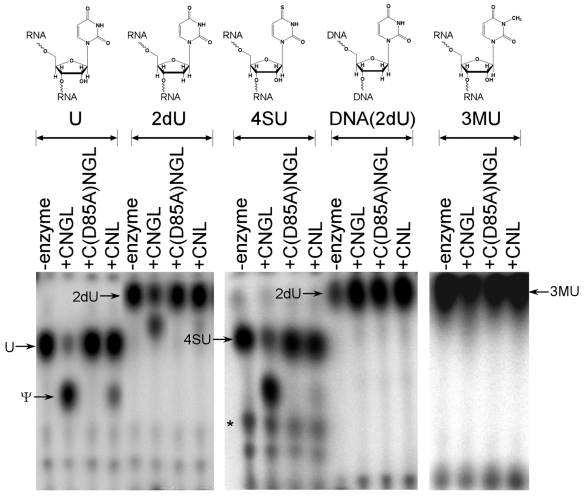

FIGURE 2: Results of enzyme activity assay of modified RNA substrates. Thin-layer chromatography radiograms of the wild-type and modified substrates following reactions with various RNP complexes. "C" denotes Cbf5, "C(D85A)" denotes the RNP containing Asp85-to-Ala mutation, "G" denotes Gar1, "N" denotes Nop10, and "L" denotes L7Ae. All reactions contain a guide RNA and a ^{32}P-labeled 22mer substrate RNA containing one of the following target nucleotide: uridine (U), 2′-deoxyuridine (2dU), 3-methyluridine (3MU), and 4-thiouridine (4SU). DNA(2dU) substrate is the same as 2dU except for that all ribonucleotides of the 22mer are replaced by deoxynucleotides.

prevented pseudouridylation, however, was unexpected because of the small perturbation on the electronic structure of uridine by the 3-methyl group.

Crystal Structures of the Nonreactive and Postreactive Complexes. A crystal structure of the nonreactive 3MU containing RNA in complex with the Pf H/ACA RNP that contains Cbf5, Nop10, L7Ae, and a guide RNA was determined and refined at 2.7 Å. Its overall structures bear strong similarity to the previously determined 5FhΨ-bound RNP structure (*15*, *16*) (Figure 3). A σA-weighted electron density map around the active site clearly revealed the presence of 3MU (Figure 3). Consistent with enzyme activity assays, electron densities showed that 3MU was not isomerized by or cross-linked to the enzyme. Therefore, this structure represents a nonreactive complex, and structural features observed in this structure represent those prior to catalysis.

The nucleobase of 3MU is bound at a location significantly different from that of the previously determined 5FhΨ (Figure 4). This location suggests two possible mechanisms responsible for its inability to be isomerized. First, the presence of the 3-methyl group sufficiently disrupts the microenvironement of the enzyme so that the nucleophilic attack on either the C1′ or C6 is blocked (Figure 4A). Second, under the assumption that 5FhΨ represents the on-path intermediate and that the 3-methyl group minimally disrupts pyrimidine electronic structure, 3MU would result in an intermediate whose 3-methyl group clashes with Asp85 (Figure 4B). Hence, the repulsive nature of the intermediate may have blocked its isomerization by the enzyme.

Our enzyme activity assay showed that both 4SU- and 2dU-containing substrates are active in pseudouridylation, and their complexes with the pseudouridine synthase, therefore, represent product complexes. Structures of the 4SU- and 2dU-containing complexes were refined at 2.3 and 2.6 Å, respectively (Figure 3). In both structures, all substrate nucleotides except the modified

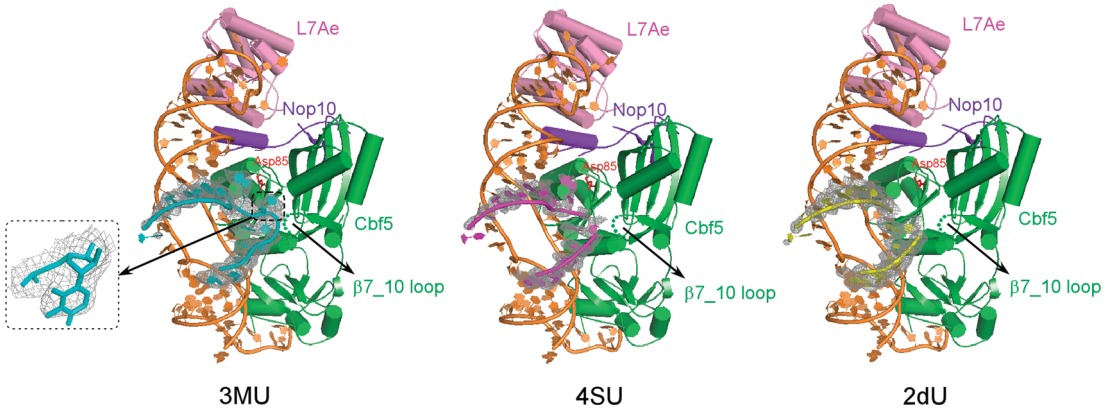

FIGURE 3: Structures of the three substrate anologue complexes with the H/ACA RNP. Electron density maps are drawn around substrate nucleotides. For 3MU, the final σ-weighted $3F_o - 2F_c$ map at 1.0σ is drawn. 3MU is in colored in cyan, 2dU in yellow, and 4SU in magenta. Note that the +1 and the target nucleotides for the 2dU complex and the target nucleotide for the 4SU complex are not modeled due to disorder.

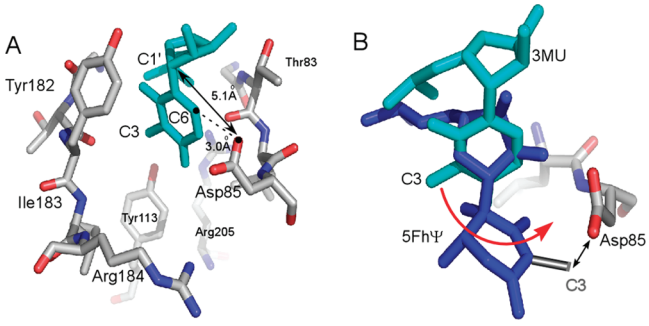

FIGURE 4: Active site geometry of 3MU substrate−RNP complexes (A) and its comparison with that of the 5FhΨ complex (B). Cbf5 is colored in gray (carbon), red (oxygen), and blue (nitrogen). The target 3MU nucleotide is colored in cyan. Enzyme−substrate interactions are indicated by dashed lines and are labeled with distances. B. The position of 5FhΨ (blue) indicates that of the potential reaction intermediate of 3MU and the close contact between the 3-methyl group (gray) and Asp85.

target uridine and the +1 nucleotide (G11) are well ordered and could be modeled into the electron density map (Figure 3). We interpret this as an indication that the enzyme active site has low affinity for the reaction products. These structures represent the postreactive state of the enzyme.

Structural Transitions and Mutational Effects of the Active Site. To the first order of approximation, we now have a complete set of structures representing prereactive (3MU), intermediate (5FhΨ), and postreactive (2dU and 4SU) enzyme complexes (Figure 5). These structures provide an unusual opportunity for us to analyze enzyme structural features before, during, and after reaction. We superimposed the catalytic domain of all structures reported here plus that of 5FhΨ reported previously (PDB: 3HJW) (Figure 5A) and compared their enzyme structures.

Core active site residues superimpose surprisingly well except for one residue. Figure 5A shows that Asp85, Tyr113, Ile183, and Arg184 have small spatial variations. Among these, Asp85 is strictly conserved while Tyr113 is nearly universally conserved except for the TruD family of pseudouridine synthases where it is phenylalanine (*28*−*37*). Ile183 can be replaced by hydrophobic residues, and Arg184 is often replaced by lysine (*30*, *34*, *36*, *38*) in all pseudouridine synthases. Interestingly, Tyr182 is the residue that has the largest variation, and it exhibits a family-dependent conservation pattern. While it is well conserved within the TruB family of pseudouridine synthases, it can be replaced by

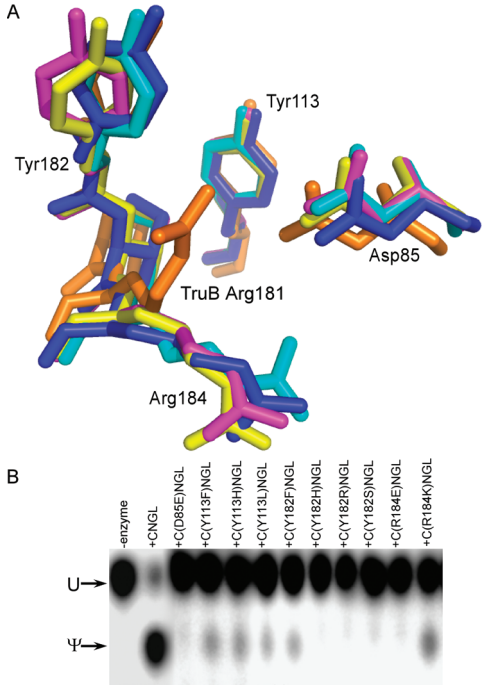

FIGURE 5: Structural changes and mutational results of the active site. (A) Superimposed core active site residues of 3MU (cyan), 5FhΨ (blue), 2dU (yellow), 4SU (magenta) complexes and TruB (gray). (B) Pseudouridylation activity assay results of the wild-type and the archaeal H/ACA RNP containing Cbf5 mutants.

histidine (*31*−*33*, *35*, *36*) or arginine (*28*, *29*, *39*) in other families of pseudouridine synthases. As Tyr182 residue directly lines the back of the target uridine, it must participate in substrate binding. Its family-dependent conservation may correlate with different substrate specificity of each enzyme. The observed structural variation among substrates of different reaction status further suggests that Tyr182 is critical to substrate binding and releasing the product when the reaction process is complete.

In order to support the observed structural data on the active site, we mutated Asp85 to glutamate (D85E), Tyr113 to phenylalanine (Y113F), histidine (Y113H), or leucine (Y113L), Tyr182 to phenylalanine (Y182F), arginine (Y182R), histidine (Y182H), or serine (Y182S), and Arg184 to glutamate (R184E) or lysine (R184K) and tested their effects on in vitro pseudouridylation. Despite their difference in structural flexibility, we found that D85E, Y182F, Y182H, Y182S, and R184E all abolished the enzyme

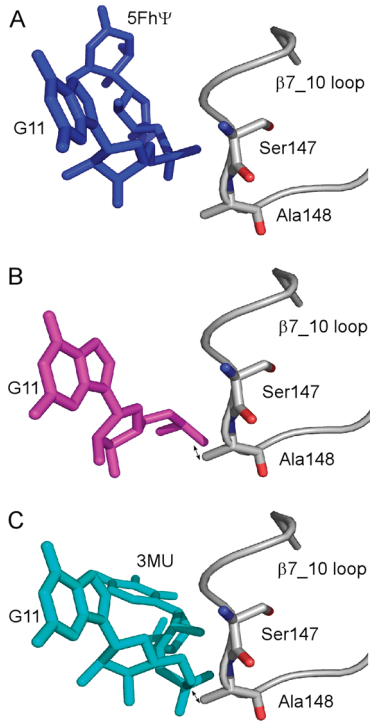

FIGURE 6: The Cbf5 β7_10 loop is sensitive to the structure of bound substrate RNA. The position of the Cbf5 β7_10 loop (gray) in the 5FhΨ structure (A, blue) is used to model its positions in the 4SU (B, magenta) and the 3MU (C, cyan) complex structures. The arrows indicate the close contact between the substrate and the loop if positioned similarly as in the 5FhΨ complex.

activity (Figure 5B). Surprisingly, all mutants of Tyr113 maintained a low level of activity (Figure 5B) in contrast to the previously demonstrated essentiality in stand alone pseudouridine synthases (*40*). We interpret this result as that the RNP pseudouridine synthase has less dependence on Tyr113. Another two mutants that maintained enzyme activity were Y182F and R184K (Figure 6B). Taken together, the RNP pseudouridine synthase minimally requires Asp85, a hydrophobic ring at position 182, and a positive charge at position 184 for the isomerization reaction.

Structural Transitions of the β7_10 Loop. The second structural difference between the nonreactive and reactive complex structures occurs on the Cbf5 β7_10 loop that had previously been described as ordered and anchoring the 5FhΨ-containing substrate RNA (*15*, *16*) (Figure 6A). In the nonreactive and postreactive structures reported here, as well as in substrate-free enzyme complex structures (*17*, *18*, *41*), this loop is not anchored to interact with the substrate (Figure 3). Correspondingly, compared to the other substrate analogues, the 5FhΨ nucleotide is bound deepest in the active site pocket and interacts most extensively with the active site network (*15*). Similarly, the +1 nucleotide (G11) is also closer to the active site than other substrates. Superimposed structures suggest that the target nucleotide in the 3MU and 4SU complex would prevent fully docking of the β7_10 loop, mostly due to a close distance between the phosphate group of the +1 nucleotide, G11, and the loop (Figure 6B,C). This comparison suggests that the β7_10 loop plays a specific role in positioning the reaction intermediate.

DISCUSSION

Elucidation of biochemical mechanisms of an enzyme requires a complete view along its functional path. This is often accomplished by obtaining high-resolution structures of enzymatic complexes that are blocked at specific chemical groups. This process may be limited to the available chemical modifications and their unknown effects on catalysis. It is, thus, crucial to combine structural data with functional investigations. Using a combined approach in this report, we identified a nonreactive and two postreactive analogues for the Pf box H/ACA RNP pseudouridine synthase. We have demonstrated that 3-methyl modification of uridine inhibited uridine isomerization while 2′-deoxy and 4-thiol modification did not. We further provided structural analysis that confirmed functional results and a putative mechanism for discrimination of 3-methyl modification by the H/ACA RNP pseudouridine synthase.

We observed structural transitions taking place among the different functional states. A substrate-binding tyrosine residue undergoes the largest changes, and its mutation reduced or abolished enzyme activity. A substrate-anchoring loop is found to be sensitive to the reaction status of the substrate and is thus an important element for substrate binding and release. The β7_10 loop of Cbf5 is only ordered when 5FhΨ, that represents reaction intermediate, is bound at the active site through interactions with the backbone of the substrate and the +1 nucleotide and is disordered when any other substrate analogue, either reactive or inactive, is used. We have previously shown by structural and fluorescence studies that the noncatalytic subunit, Gar1, has the ability to modulate the orientation of this loop (*15*, *42*). These findings further implicate a switch-like mechanism mediated by the Cbf5 β7_10 loop and Gar1 in the pseudouridylation pathway.

Our enzyme activity assays on the three substrates containing modified uridine provide some insights on the catalytic strategy of the H/ACA RNP pseudouridine synthase. In general, our knowledge on the catalytic mechanism of the pseudouridylation reaction is limited. The essential role played by the strictly conserved Asp has been demonstrated in many pseudouridine synthases. However, the catalytic strategy facilitated by Asp remains elusive. The fact that 2′-deoxy modification of the target uridine did not inhibit isomerization ruled out a direct role of the 2′-hydroxyl group in catalysis despite that it is placed near Asp. On the other hand, the fact that 3-methyluridine prevented isomerization suggests a role played by the pyrimidine ring in catalysis. This interpretation is consistent with but not a proof of the previously proposed Michael addition mechanism (*43*, *44*). Elucidation of the catalytic mechanism of pseudouridine synthases requires additional structural and mechanistic studies.

SUPPORTING INFORMATION AVAILABLE

A figure showing the successfully ligated products from the DNA splint method. This material is available free of charge via the Internet at http://pubs.acs.org.

REFERENCES

1. Balakin, A. G., Smith, L., and Fournier, M. J. (1996) The RNA world of the nucleolus: two major families of small RNAs defined by different box elements with related functions. *Cell 86* (5), 823–834.
2. Ganot, P., Bortolin, M. L., and Kiss, T. (1997) Site-specific pseudouridine formation in preribosomal RNA is guided by small nucleolar RNAs. *Cell 89* (5), 799–809.
3. Decatur, W. A., and Fournier, M. J. (2003) RNA-guided nucleotide modification of ribosomal and other RNAs. *J. Biol. Chem. 278* (2), 695–698.
4. Baker, D. L., Youssef, O. A., Chastkofsky, M. I., Dy, D. A., Terns, R. M., and Terns, M. P. (2005) RNA-guided RNA modification: functional organization of the archaeal H/ACA RNP. *Genes Dev. 19* (10), 1238–1248.
5. Meier, U. T. (2005) The many facets of H/ACA ribonucleoproteins. *Chromosoma 114* (1), 1–14.

6. Heiss, N. S., Knight, S. W., Vulliamy, T. J., Klauck, S. M., Wiemann, S., and Mason, P. J.; et al. (1998) X-linked dyskeratosis congenita is caused by mutations in a highly conserved gene with putative nucleolar functions. *Nat. Genet. 19* (1), 32–38.
7. Vulliamy, T., Marrone, A., Goldman, F., Dearlove, A., Bessler, M., and Mason, P. J.; et al. (2001) The RNA component of telomerase is mutated in autosomal dominant dyskeratosis congenita. *Nature 413* (6854), 432–435.
8. Walne, A. J., Vulliamy, T., Marrone, A., Beswick, R., Kirwan, M., and Masunari, Y.; et al. (2007) Genetic heterogeneity in autosomal recessive dyskeratosis congenita with one subtype due to mutations in the telomerase-associated protein NOP10. *Hum. Mol. Genet. 16* (13), 1619–1629.
9. Vulliamy, T., Beswick, R., Kirwan, M., Marrone, A., Digweed, M., and Walne, A.; et al. (2008) Mutations in the telomerase component NHP2 cause the premature ageing syndrome dyskeratosis congenita. *Proc. Natl. Acad. Sci. U.S.A. 105* (23), 8073–8078.
10. Huang, L., Pookanjanatavip, M., Gu, X., and Santi, D. V. (1998) A conserved aspartate of tRNA pseudouridine synthase is essential for activity and a probable nucleophilic catalyst. *Biochemistry 37* (1), 344–351.
11. Longley, D. B., Harkin, D. P., and Johnston, P. G. (2003) 5-fluorouracil: mechanisms of action and clinical strategies. *Nat. Rev. Cancer 3* (5), 330–338.
12. Greenhalgh, D. A., and Parish, J. H. (1990) Effect of 5-fluorouracil combination therapy on RNA processing in human colonic carcinoma cells. *Br. J. Cancer 61* (3), 415–419.
13. Greenhalgh, D. A., and Parish, J. H. (1989) Effects of 5-fluorouracil on cytotoxicity and RNA metabolism in human colonic carcinoma cells. *Cancer Chemother. Pharmacol. 25* (1), 37–44.
14. Fang, F., Hoskins, J., and Butler, J. S. (2004) 5-fluorouracil enhances exosome-dependent accumulation of polyadenylated rRNAs. *Mol. Cell. Biol. 24* (24), 10766–10776.
15. Liang, B., Zhou, J., Kahen, E., Terns, R. M., Terns, M. P., and Li, H. (2009) Structure of a functional ribonucleoprotein pseudouridine synthase bound to a substrate RNA. *Nat. Struct. Mol. Biol. 16* (7), 740–746.
16. Duan, J., Li, L., Lu, J., Wang, W., and Ye, K. (2009) Structural mechanism of substrate RNA recruitment in H/ACA RNA-guided pseudouridine synthase. *Mol. Cell 34* (4), 427–439.
17. Rashid, R., Liang, B., Baker, D. L., Youssef, O. A., He, Y., and Phipps, K.; et al. (2006) Crystal structure of a Cbf5-Nop10-Gar1 complex and implications in RNA-guided pseudouridylation and dyskeratosis congenita. *Mol. Cell 21* (2), 249–260.
18. Li, L., and Ye, K. (2006) Crystal structure of an H/ACA box ribonucleoprotein particle. *Nature 443* (7109), 302–307.
19. Charpentier, B., Muller, S., and Branlant, C. (2005) Reconstitution of archaeal H/ACA small ribonucleoprotein complexes active in pseudouridylation. *Nucleic Acids Res. 33* (10), 3133–3144.
20. McKenna, S. A., Kim, I., Puglisi, E. V., Lindhout, D. A., Aitken, C. E., and Marshall, R. A.; et al. (2007) Purification and characterization of transcribed RNAs using gel filtration chromatography. *Nat. Protoc. 2* (12), 3270–3277.
21. Zbyszek Otwinowski, W. M. (1997) Processing of X-ray diffraction data collected in oscillation mode. *Methods Enzymol.* 307–326.
22. Vagin, A., and Teplyakov, A. (1997) MOLREP: an automated program for molecular replacement. *J. Appl. Crystallogr. 30*, 1022–1025.
23. Emsley, P., and Cowtan, K. (2004) Coot: model-building tools for molecular graphics. *Acta Crystallogr., Sect. D: Biol. Crystallogr. 60* (Part 12), 2126–2132.
24. Jones, T. A., Zou, J. Y., Cowan, S. W., and Kjeldgaard, M. (1991) Improved methods for building protein models in electron density maps and the location of errors in these models. *Acta Crystallogr. A 47* (Part 2), 110–119.
25. Adams, P. D., Grosse-Kunstleve, R. W., Hung, L. W., Ioerger, T. R., McCoy, A. J., and Moriarty, N. W.; et al. (2002) PHENIX: building new software for automated crystallographic structure determination. *Acta Crystallogr., Sect. D: Biol. Crystallogr. 58* (Part 11), 1948–1954.
26. Delano W. L. (2002) The PyMOL Molecular Graphics System (http://www.pymol.org).
27. Moore, M. J., and Sharp, P. A. (1992) Site-specific modification of pre-mRNA: the 2′-hydroxyl groups at the splice sites. *Science 256* (5059), 992–997.
28. Alian, A., DeGiovanni, A., Griner, S. L., Finer-Moore, J. S., and Stroud, R. M. (2009) Crystal structure of an RluF-RNA complex: a base-pair rearrangement is the key to selectivity of RluF for U2604 of the ribosome. *J. Mol. Biol. 388* (4), 785–800.
29. Pan, H., Ho, J. D., Stroud, R. M., and Finer-Moore, J. (2007) The crystal structure of *E. coli* rRNA pseudouridine synthase RluE. *J. Mol. Biol. 367* (5), 1459–1470.
30. McCleverty, C. J., Hornsby, M., Spraggon, G., and Kreusch, A. (2007) Crystal structure of human Pus10, a novel pseudouridine synthase. *J. Mol. Biol. 373* (5), 1243–1254.
31. Hoang, C., Chen, J., Vizthum, C. A., Kandel, J. M., Hamilton, C. S., and Mueller, E. G.; et al. (2006) Crystal structure of pseudouridine synthase RluA: indirect sequence readout through protein-induced RNA structure. *Mol. Cell 24* (4), 535–545.
32. Dong, X., Bessho, Y., Shibata, R., Nishimoto, M., Shirouzu, M., and Kuramitsu, S.; et al. (2006) Crystal structure of tRNA pseudouridine synthase TruA from *Thermus thermophilus* HB8. *RNA Biol. 3* (3), 115–122.
33. Sivaraman, J., Iannuzzi, P., Cygler, M., and Matte, A. (2004) Crystal structure of the RluD pseudouridine synthase catalytic module, an enzyme that modifies 23S rRNA and is essential for normal cell growth of *Escherichia coli*. *J. Mol. Biol. 335* (1), 87–101.
34. Kaya, Y., Del Campo, M., Ofengand, J., and Malhotra, A. (2004) Crystal structure of TruD, a novel pseudouridine synthase with a new protein fold. *J. Biol. Chem. 279* (18), 18107–18110.
35. Del Campo, M., Ofengand, J., and Malhotra, A. (2004) Crystal structure of the catalytic domain of RluD, the only rRNA pseudouridine synthase required for normal growth of *Escherichia coli*. *RNA 10* (2), 231–239.
36. Sivaraman, J., Sauve, V., Larocque, R., Stura, E. A., Schrag, J. D., and Cygler, M.; et al. (2002) Structure of the 16S rRNA pseudouridine synthase RsuA bound to uracil and UMP. *Nat. Struct. Biol. 9* (5), 353–358.
37. Hoang, C., and Ferre-D'Amare, A. R. (2001) Cocrystal structure of a tRNA Psi55 pseudouridine synthase: nucleotide flipping by an RNA-modifying enzyme. *Cell 107* (7), 929–939.
38. Hoang, C., and Ferre-D'Amare, A. R. (2004) Crystal structure of the highly divergent pseudouridine synthase TruD reveals a circular permutation of a conserved fold. *RNA 10* (7), 1026–1033.
39. Sunita, S., Zhenxing, H., Swaathi, J., Cygler, M., Matte, A., and Sivaraman, J. (2006) Domain organization and crystal structure of the catalytic domain of *E.coli* RluF, a pseudouridine synthase that acts on 23S rRNA. *J. Mol. Biol. 359* (4), 998–1009.
40. Phannachet, K., Elias, Y., and Huang, R. H. (2005) Dissecting the roles of a strictly conserved tyrosine in substrate recognition and catalysis by pseudouridine 55 synthase. *Biochemistry 44* (47), 15488–15494.
41. Liang, B., Xue, S., Terns, R. M., Terns, M. P., and Li, H. (2007) Substrate RNA positioning in the archaeal H/ACA ribonucleoprotein complex. *Nat. Struct. Mol. Biol. 14*, 1189–1195.
42. Liang, B., Kahen, E. J., Calvin, K., Zhou, J., Blanco, M., and Li, H. (2008) Long-distance placement of substrate RNA by H/ACA proteins. *RNA 14* (10), 2086–2094.
43. Kammen, H. O., Marvel, C. C., Hardy, L., and Penhoet, E. E. (1988) Purification, structure, and properties of *Escherichia coli* tRNA pseudouridine synthase I. *J. Biol. Chem. 263* (5), 2255–2263.
44. Gu, X. R., Liu, Y. Q., and Santi, D. V. (1999) The mechanism of pseudouridine synthase I as deduced from its interaction with 5-fluorouracil-tRNA. *Proc. Natl. Acad. Sci. U.S.A. 96* (25), 14270–14275.

Supplementary information

Functional and structural consequences of uridine substitutions on H/ACA ribonucleoprotein particle pseudouridine synthase

Jing Zhou[1], Bo Liang[2], & Hong Li[1,2]

[1]Department of Chemistry and Biochemistry, [2]Institute of Molecular Biophysics, Florida State University, Tallahassee, FL 32306, USA.

Correspondence and requests for materials should be addressed to H.L.

Email: hong.li@fsu.edu Phone: (850) 644-6785 Fax: (850) 644-7244

Supplementary Figure S1

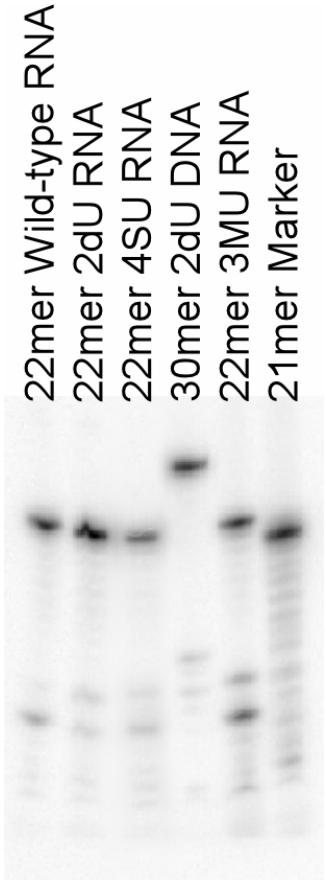

Figure S1 Legend. SDS-PAGE gel analysis of ligated products of halfmer RNA substrates containing modified uridine in place of the target uridine.